Обзор ArXiv: astro-ph, 30 мая – 3 июня 2016

От Сильченко О.К.

Astro-ph: 1605.08845

The effect of environment on the structure of disk galaxies

Florian Pranger[1]★, Ignacio Trujillo[2,3], Lee S. Kelvin[4], María Cebrián[2,3]
[1]*National Astronomical Research Institute of Thailand, 191 Huay Kaew Road, 50200 Chiang Mai, Thailand*
[2]*Instituto de Astrofísica de Canarias, c/Vía Láctea s/n, E-38205-La Laguna, Tenerife, Spain*
[3]*Departamento de Astrofísica, Universidad de La Laguna, E-38205 La Laguna, Tenerife, Spain*
[4]*Astrophysics Research Institute, Liverpool John Moores University, IC2, Liverpool Science Park, 146 Brownlow Hill, Liverpool L3 5RF, UK*

31 May 2016

ABSTRACT

We study the influence of environment on the structure of disk galaxies, using IMFIT to measure the g- and r-band parameters of the surface-brightness profiles for ~200 low-redshift (z<0.051) cluster and field disk-galaxies with intermediate stellar mass (10^{10} $M_{\odot}$ < $M_{\star}$ < 4×10^{10} $M_{\odot}$) from the Sloan Digital Sky Survey, DR7. Based on this measurement, we

Выборка

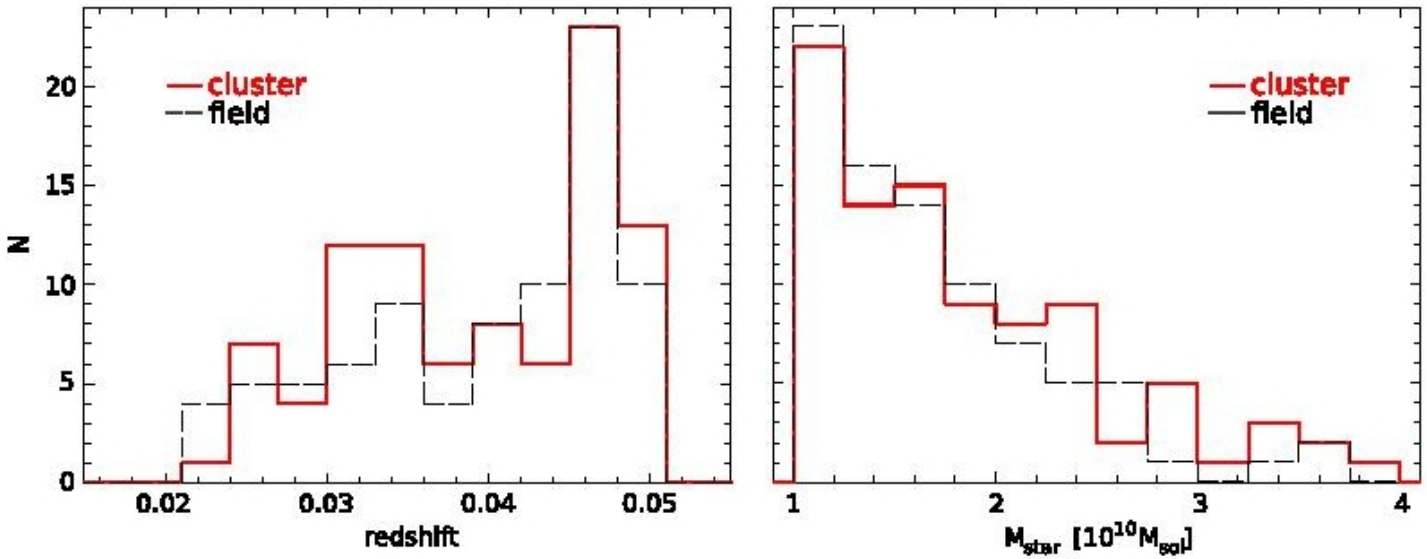

Figure 1. *Left panel:* redshift distribution of the total cluster and total field sample. *right panel:* Distribution of stellar mass for the total cluster and total field sample.

Примеры

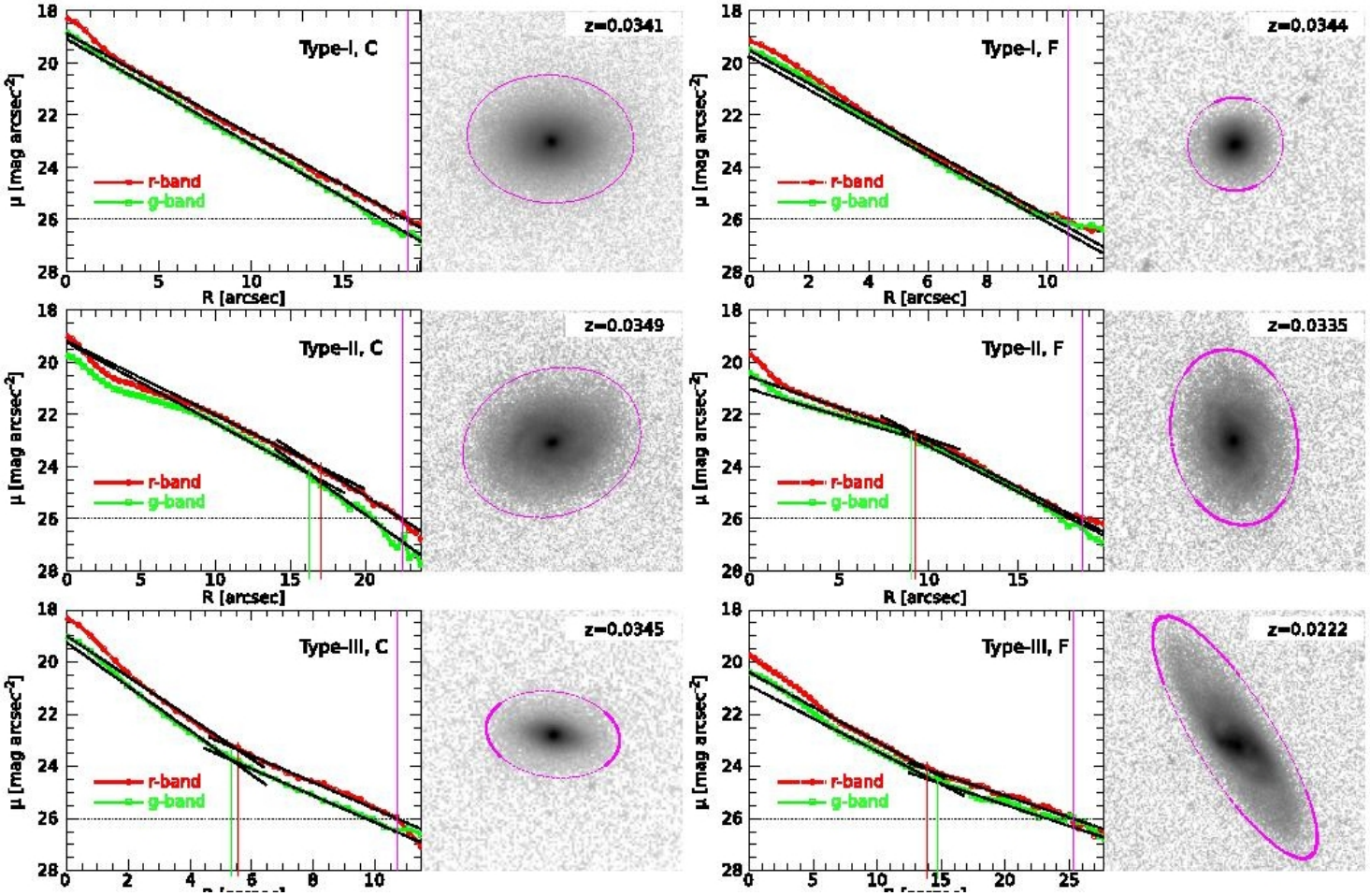
Type-I, C
z=0.0341
Type-I, F
z=0.0344
Type-II, C
z=0.0349
Type-II, F
z=0.0335
Type-III, C
z=0.0345
Type-III, F
z=0.0222
r-band
g-band
μ [mag arcsec⁻²]
R [arcsec]

Результаты

	Cluster				Field			
Sample	Type-I	Type-II	Type-III	TCS	Type-I	Type-II	Type-III	TFS
N	14±4	53±7	25±5	92	5±2	54±7	25±5	84
%	15±4	58±8	27±5	100	6±2	64±8	30±6	100
R_e [kpc]	2.43±0.13	2.79±0.12	2.01±0.10	2.50±0.08	2.53±0.03 (±0.36)	3.21±0.12	2.37±0.18	2.79±0.10
n	2.04±0.06	1.81±0.05	2.27±0.04	1.96±0.03	1.73±0.09 (±0.23)	1.84±0.04	2.01±0.06	1.87±0.03
$M_\star$ [$10^{10} M_\odot$]	1.85±0.38	1.53±0.07	2.10±0.14	1.67±0.09	1.65±0.07 (±0.39)	1.76±0.07	1.61±0.08	1.65±0.05
$(g-r)_{in}$	0.498±0.040	0.364±0.017	0.516±0.020	-	0.224±0.041 (±0.099)	0.243±0.018	0.376±0.028	-
$(g-r)_{in,1}$	0.478±0.032	0.335±0.018	0.505±0.018	-	0.213±0.034 (±0.084)	0.216±0.019	0.351±0.029	-
$(g-r)_{in,2}$	0.468±0.033	0.316±0.016	0.496±0.016	-	0.205±0.017 (±0.074)	0.197±0.017	0.346±0.028	-
$(g-r)_{out}$	-	0.293±0.020	0.487±0.024	-	-	0.155±0.019	0.344±0.029	-
$h_{1,g}$ [kpc]	1.73±0.08	2.43±0.13	1.27±0.08	-	1.42±0.10 (±0.26)	2.69±0.27	1.29±0.09	-
$h_{2,g}$ [kpc]	- " -	1.42±0.05	2.01±0.12	-	- " -	1.33±0.04	1.80±0.07	-
$ratio_g$	1	1.79±0.10	0.63±0.02	-	1	1.94±0.28	0.76±0.04	-
$R_{b,g}$ [kpc]	-	4.69±0.22	4.41±0.29	-	-	5.32±0.23	3.87±0.28	-
$h_{1,r}$ [kpc]	1.68±0.12	2.41±0.09	1.25±0.06	-	1.42±0.11 (±0.30)	2.34±0.21	1.20±0.10	-
$h_{2,r}$ [kpc]	- " -	1.42±0.05	2.11±0.13	-	- " -	1.31±0.05	1.84±0.10	-
$ratio_r$	1	1.62±0.05	0.59±0.03	-	1	1.89±0.16	0.69±0.04	-
$R_{b,r}$ [kpc]	-	5.43±0.22	4.21±0.26	-	-	5.28±0.24	4.05±0.30	-

Результаты

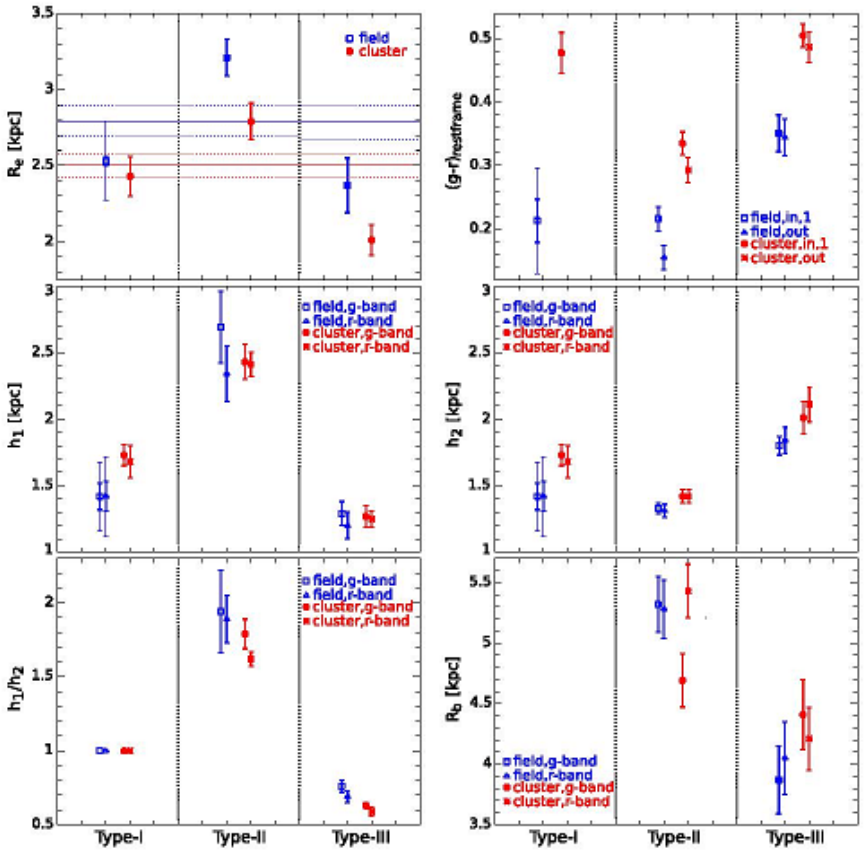

Figure 3. Median galaxy properties for both environments and all three surface-brightness profile types. Errors are 1-sigma bootstrap estimates. Thin error bars indicate the standard deviation values for the smallest sample of Type-I field galaxies. *Top row:* effective radius, R_e, and $(g-r)_{restframe}$ colour. For Type-II and Type-III galaxies, $(g-r)_{in,1}$ and $(g-r)_{out}$ are plotted. For Type-I galaxies, we plot only $(g-r)_{in,1}$, which in this case is the colour measured in the entire disk region (bulge masked at 0.5 R_e). The horizontal lines in the first panel indicate the median R_e (and bootstrap errors) for the total cluster and field sample, respectively. *Middle row:* inner (h_1) and outer (h_2) exponential scalelength for both measured bands. *Bottom row:* Scalelength ratio (h_1/h_2) and break radius (R_b) for both measured bands. For Type-I galaxies, the break radius is not defined and the scalelength ratio is by definition equal to unity.

Astro-ph: 1606.00009

KINEMATIC DOWNSIZING AT $z\sim 2$

Raymond C. Simons[1], Susan A. Kassin[2], Jonathan R. Trump[3†], Benjamin J. Weiner[4], Timothy M. Heckman[1], Guillermo Barro[5], David C. Koo[6], Yicheng Guo[6], Camilla Pacifici[7^], Anton Koekemoer[2], and Andrew W. Stephens[8]

[1]Johns Hopkins University, Baltimore, MD, 21218, USA; rsimons@jhu.edu
[2]Space Telescope Science Institute, 3700 San Martin Drive, Baltimore, MD, 21218, USA
[3]Department of Astronomy and Astrophysics and Institute for Gravitation and the Cosmos, 525 Davey Lab, The Pennsylvania State University, University Park, PA 16802, USA
[4]Steward Observatory, 933 N. Cherry St, University of Arizona, Tucson, AZ 85721, USA
[5]Department of Astronomy, University of California Berkeley, 501 Campbell Hall, Berkeley, CA 94720, USA
[6]UCO/Lick Observatory, Department of Astronomy and Astrophysics, University of California, Santa Cruz, CA 95064, USA
[7]Astrophysics Science Division, Goddard Space Flight Center, Code 665, Greenbelt, MD 20771, USA
[8]Gemini Observatory, Northern Operations Center, 670 N A'ohoku Place, Hilo, HI 96720
[†]Hubble Fellow
[^]NASA Postdoctoral Program Fellow

Draft version June 2, 2016

ABSTRACT

We present results from a survey of the internal kinematics of 49 star-forming galaxies at $z \sim 2$ in the CANDELS fields with the Keck/MOSFIRE spectrograph (SIGMA, Survey in the near-Infrared of Galaxies with Multiple position Angles). Kinematics (rotation velocity V_{rot} and integrated gas velocity dispersion σ_g) are measured from nebular emission lines which trace the hot ionized gas surrounding star-forming regions. We find that by $z \sim 2$, massive star-forming galaxies ($\log M_*/M_\odot \gtrsim 10.2$) have assembled primitive disks: their kinematics are dominated by rotation, they are consistent with a marginally stable disk model, and they form a Tully-Fisher relation. These massive galaxies have values of V_{rot}/σ_g which are factors of 2–5 lower than local well-ordered galaxies at similar masses. Such results are consistent with findings by other studies. We find that low mass galaxies ($\log M_*/M_\odot \lesssim 10.2$) at this epoch are still in the early stages of disk assembly: their kinematics are often supported by gas velocity dispersion and they fall from the Tully-Fisher relation to significantly low values of V_{rot}. This "kinematic downsizing" implies that the process(es) responsible for disrupting disks at $z \sim 2$ have a stronger effect and/or are more active in low mass systems. In conclusion, we

Из одномерных разрезов - карты

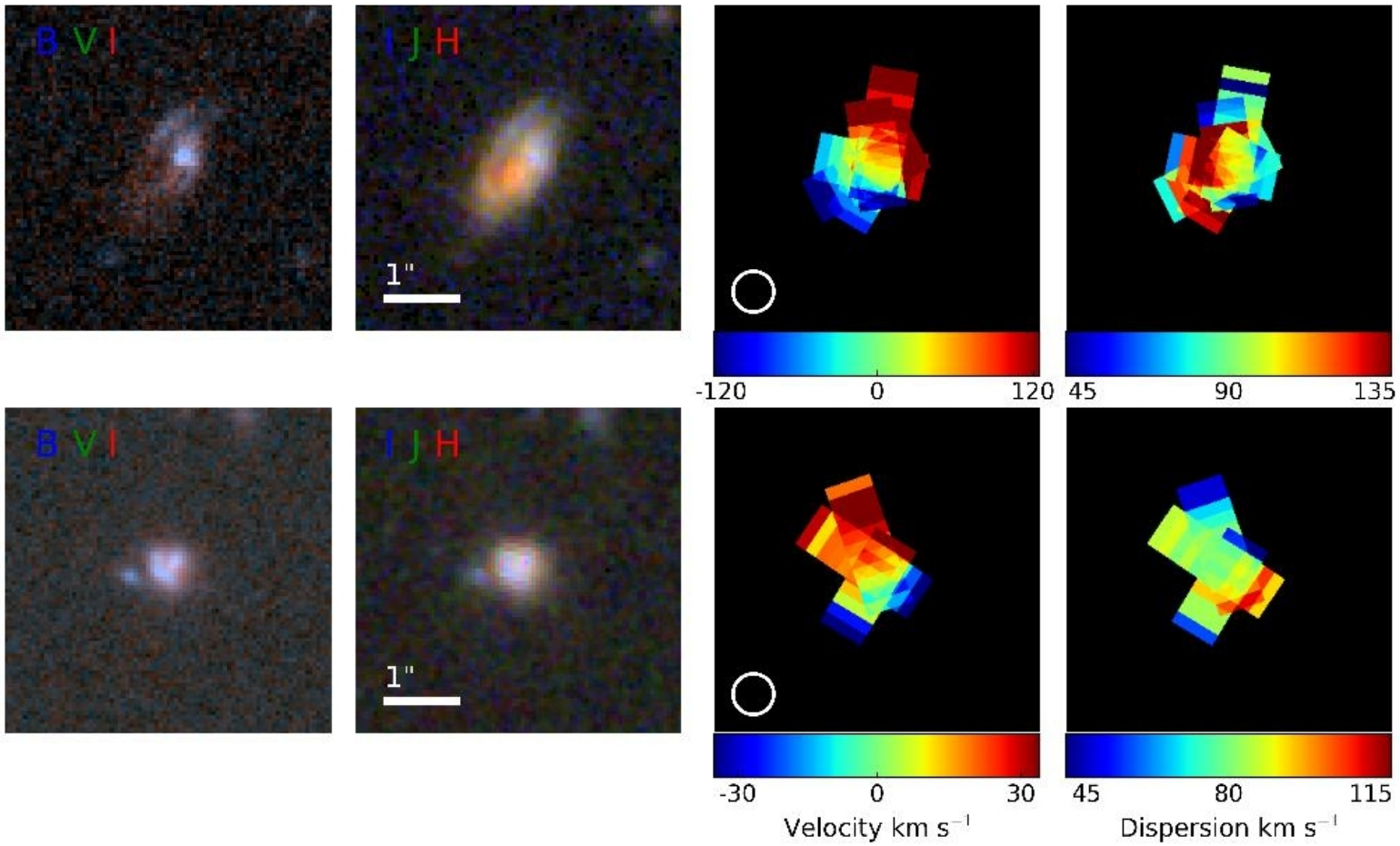

Три типа по кинематике и уроды

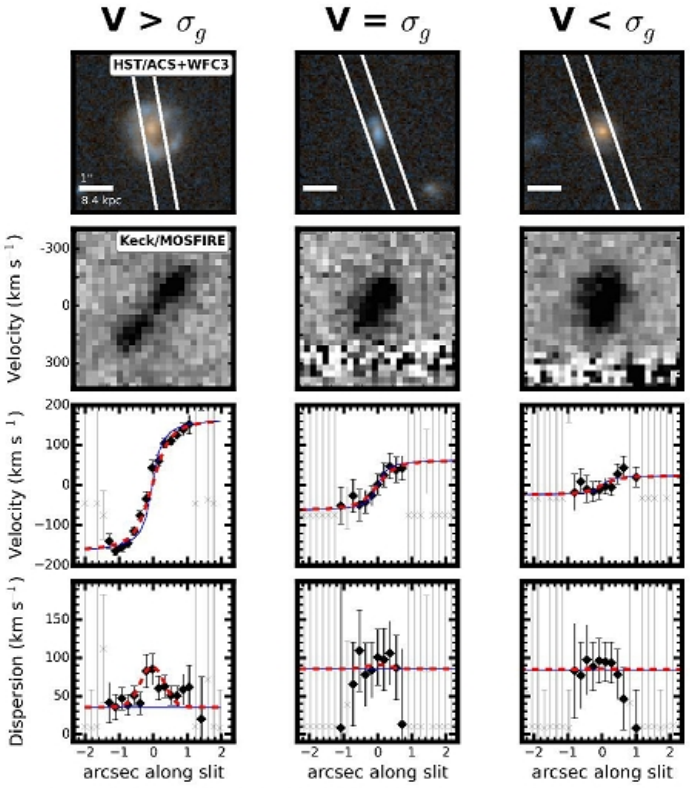

FIG. 3.— Example single slit observations are presented for three SIGMA galaxies (ID: 16600, 16209, 14602). These galaxies span the kinematic types in our sample: a rotation dominated galaxy (left column), a galaxy with equal contributions of rotation and dispersion (middle column), and a dispersion dominated galaxy (right column). In the top two rows we show the I+H-band HST/ACS-WFC3 color images with the MOSFIRE slit placement and the 2-D spectra centered around the Hα line. Strong NIR atmospheric lines are present in the middle and right columns. In the bottom two rows we show the kinematic model fits to the emission lines. The black filled diamonds represent the gaussian fits to the velocity and velocity dispersion in each row of each spectrum. The grey points are poor fits and are discarded. The best-fit models are shown as red solid lines and the intrinsic (pre-seeing blurred) models are shown as blue dashed lines. All of the rows are spatially aligned and each panel is 4.5″ on a side. Kinematic fits for all of the SIGMA galaxies are available in the Appendix.

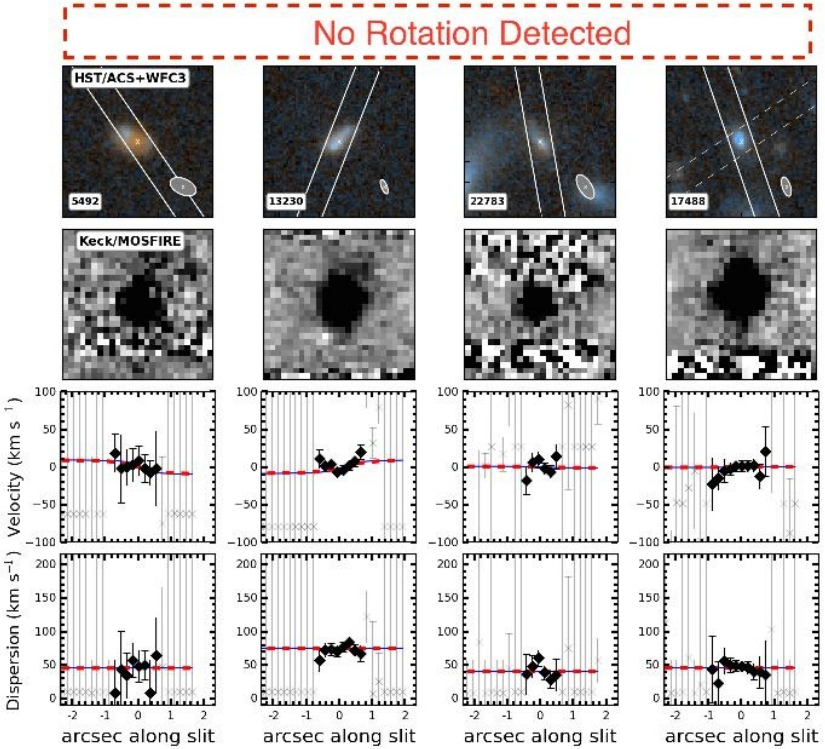

Выборка и Талли-Фишер

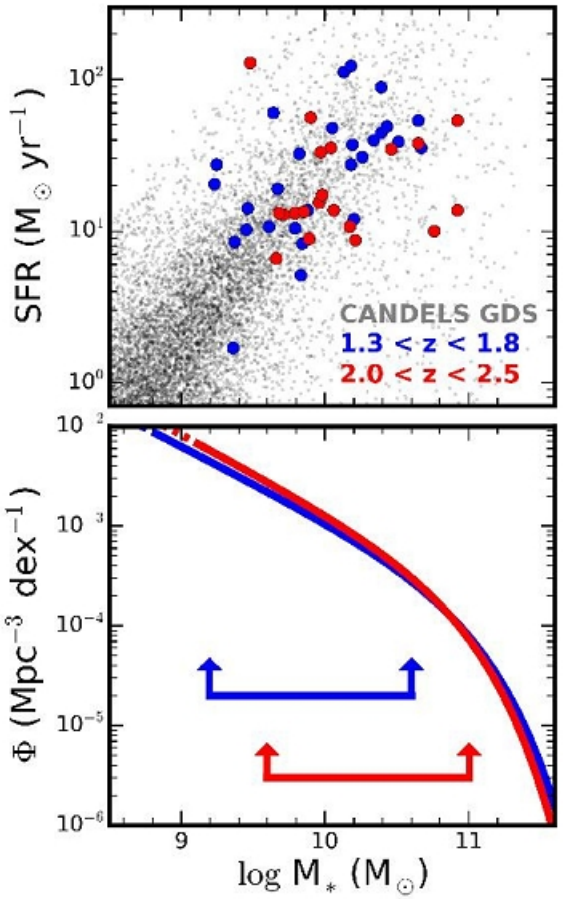

FIG. 1.— Galaxies in SIGMA (large filled points) lie along the star-formation main sequence down to a stellar mass of $\log M_*/M_\odot = 9.2$ at $z \sim 1.5$ and $\log M_*/M_\odot = 9.6$ at $z \sim 2.3$.

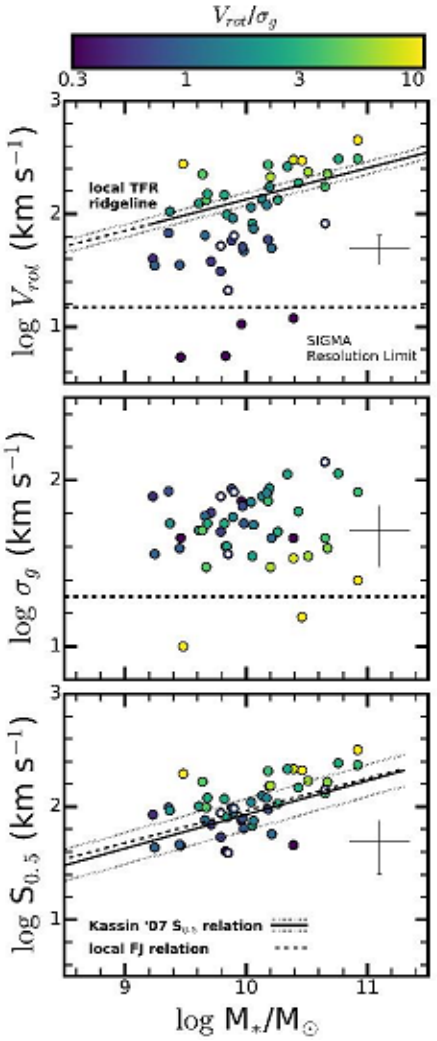

Результаты

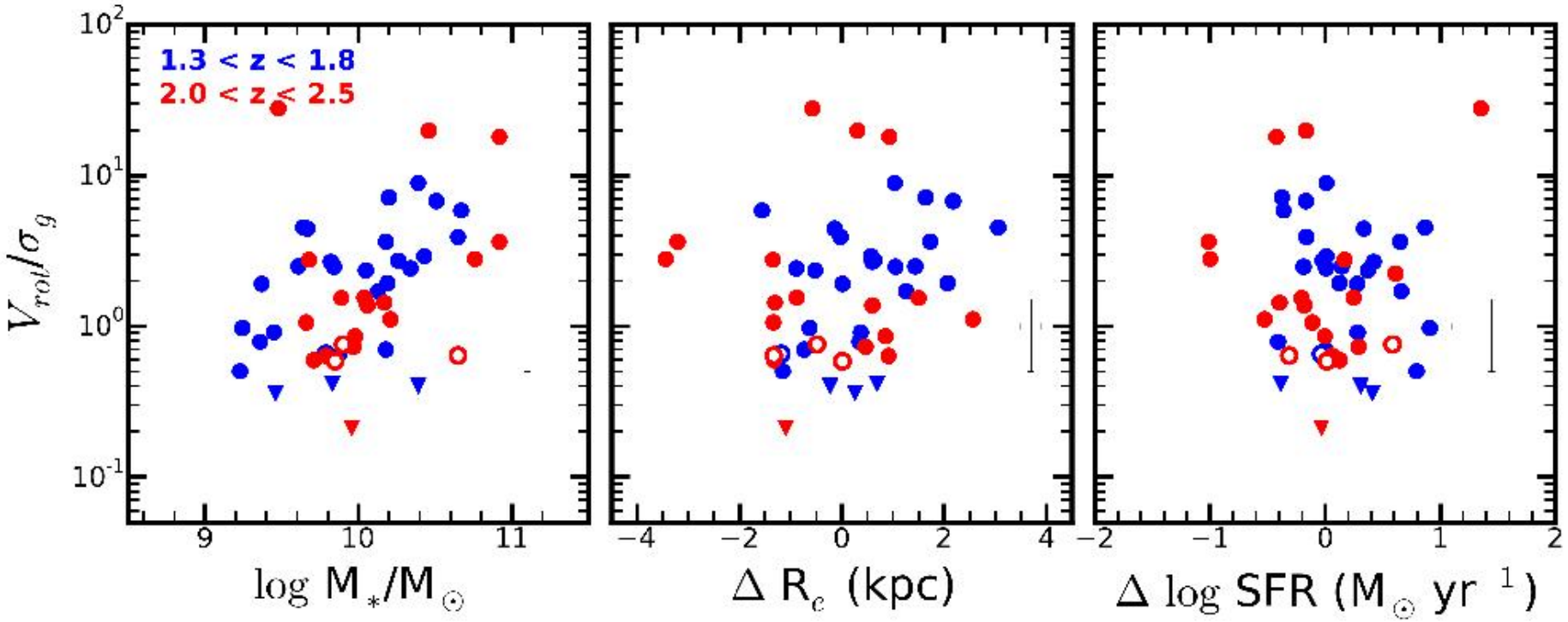

G. 6.— The kinematic order (V_{rot}/σ_g) of SIGMA galaxies is strongly correlated with stellar mass (M_*; left panel), moderately correlated
h H-band continuum size at fixed a stellar mass (ΔR_e; middle panel) and weakly correlated with with star-formation rate at fixed stella
ss (Δ log SFR; right panel). In the 3 panels we show V_{rot}/σ_g versus M_*, residuals from the $z \sim 2$ SFR-M_* relation and residuals from
$z \sim 1.75$ and $z \sim 2.25$ size-mass relations. The blue and red points represent our low and high redshift subsamples, respectively

Маржинально устойчивы массивные?

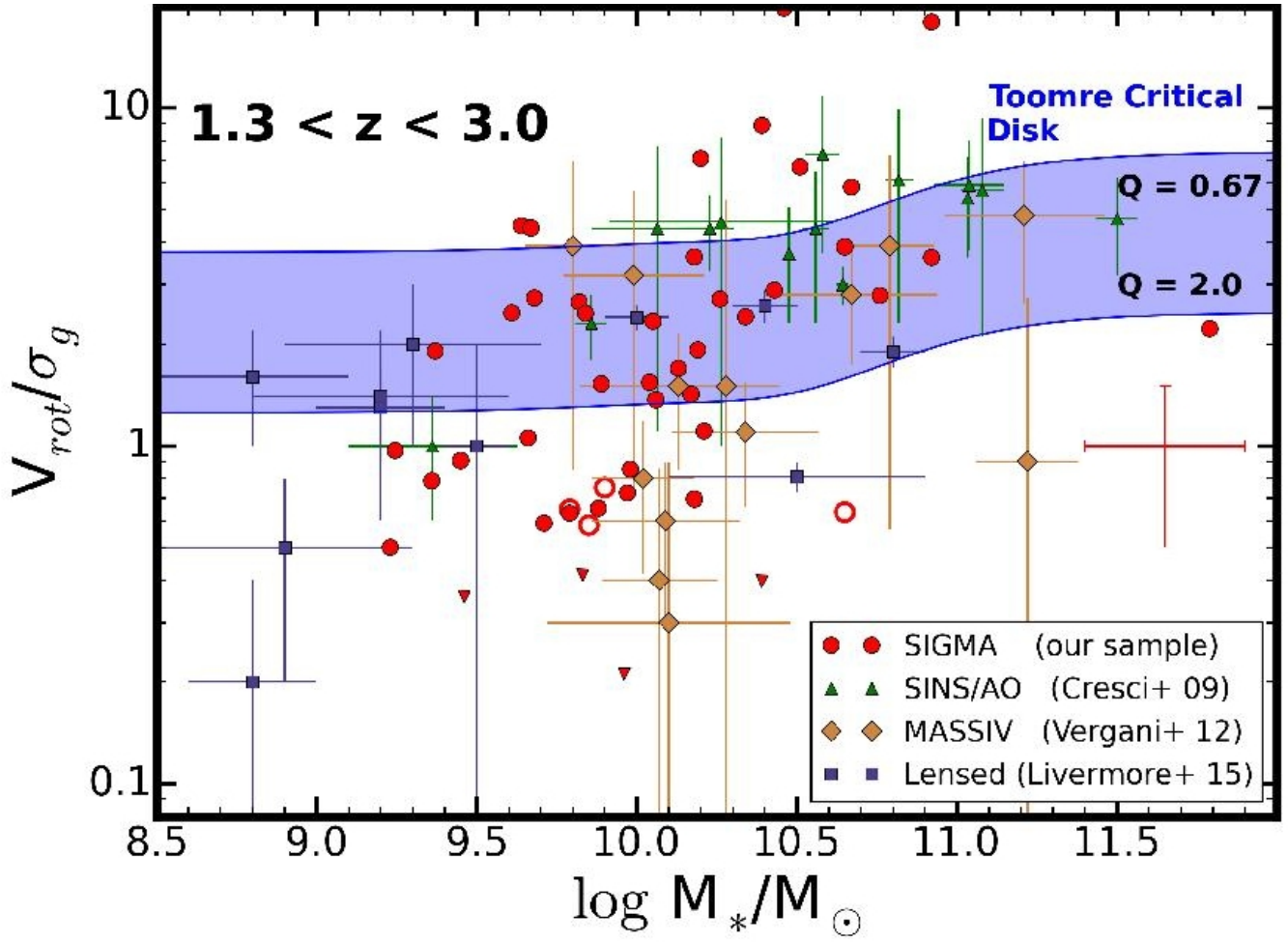

Astro-ph: 1606.00018

MEGAMASER DISKS REVEAL A BROAD DISTRIBUTION IN BLACK HOLE MASS IN SPIRAL GALAXIES

J. E. GREENE[1], A. SETH[2], M. KIM[3], R. LÄSKER, A. GOULDING[1], F. GAO[6], J. A. BRAATZ[4], C. HENKEL[5], J. CONDON[4], K. Y. LO[4], W. ZHAO

Draft version June 2, 2016

ABSTRACT

We use new precision measurements of black hole masses from water megamaser disks to investigate scaling relations between macroscopic galaxy properties and supermassive black hole (BH) mass. The megamaser-derived BH masses span $10^6 - 10^8\,M_\odot$, while all the galaxy properties that we examine (including stellar mass, bulge mass, central velocity dispersion, circular velocity) lie within a narrower range. Thus, no galaxy property correlates tightly with $M_{\rm BH}$ in $\sim L^*$ spiral galaxies. Of them all, stellar velocity dispersion provides the tightest relation, but at fixed σ_* the mean megamaser $M_{\rm BH}$ are offset by -0.6 ± 0.1 dex relative to early-type galaxies. Spiral galaxies with non-maser dynamical BH masses do not show this offset. At low mass, we do not yet know the full distribution of BH mass at fixed galaxy property; the non-maser dynamical measurements may miss the low-mass end of the BH distribution due to inability to resolve their spheres of influence and/or megamasers may preferentially occur in lower-mass BHs.

Мегамазеры!

Table 1. Galaxy Sample

Galaxy (1)	D (2)	Type (3)	M_{BH} (4)	σ^* (5)	M_{bst} (6)	M_{1kpc} (7)	Meth (8)
Mrk1029	124.0	3p	6.28± 0.13	2.12± 0.05	10.57± 0.05	10.08± 0.06	maser
NGC1320	49.1	3p	6.74± 0.16	2.15± 0.05	···	···	maser
J0437+2456	66.0	3p	6.45± 0.03	2.04± 0.05	10.57± 0.22	10.04± 0.04	maser
ESO558−G009	102.5	3p	7.22± 0.03	2.23± 0.05	···	···	maser
UGC6093	150.0	3p	7.41± 0.02	2.19± 0.05	11.21± 0.05	10.19± 0.08	maser
NGC5495	93.1	3p	7.00± 0.05	2.22± 0.05	···	···	maser
NGC5765b	113.0	3p	7.64± 0.05	2.21± 0.05	···	···	maser
IC2560	41.8	3	6.64± 0.06	2.15± 0.03	···	···	maser
NGC1068	15.9	3p	6.92± 0.25	2.18± 0.02	10.42± 0.58	10.63± 0.06	maser
NGC1194	58.0	2	7.85± 0.05	2.17± 0.07	10.81± 0.08	10.19± 0.09	maser
NGC2273	29.5	3p	6.93± 0.04	2.10± 0.03	···	···	maser
UGC3789	49.9	3p	6.99± 0.09	2.03± 0.05	···	···	maser
NGC2960	67.1	2p	7.03± 0.05	2.22± 0.04	10.98± 0.03	10.40± 0.03	maser
NGC3079	15.9	3p	6.40± 0.05	2.16± 0.02	10.38± 0.05	9.85± 0.09	maser
NGC3393	49.2	3p	7.20± 0.33	2.17± 0.03	···	···	maser
NGC4258	7.3	3	7.58± 0.03	2.06± 0.04	10.52± 0.04	10.00± 0.05	maser
Circinus	2.8	3p	6.06± 0.10	1.90± 0.02	···	···	maser
NGC4388	16.5	3p	6.86± 0.04	2.00± 0.04	10.43± 0.05	9.73± 0.06	maser
NGC4594	9.9	3	8.82± 0.05	2.38± 0.02	10.90± 0.04	10.60± 0.03	maser
NGC6264	147.6	3p	7.49± 0.05	2.20± 0.04	11.01± 0.09	9.92± 0.08	maser
NGC6323	113.4	3p	7.00± 0.05	2.20± 0.07	11.03± 0.09	9.97± 0.05	maser
MW	0.008	3p	6.63± 0.05	2.02± 0.08	···	···	star
NGC0221	0.8	1	6.39± 0.19	1.89± 0.02	···	···	star
NGC0224	0.8	3	8.15± 0.16	2.23± 0.02	···	···	star
NGC0307	52.8	2	8.60± 0.06	2.31± 0.01	10.81± 0.04	10.38± 0.03	star

Сравнение с динамически определенными M(BH)

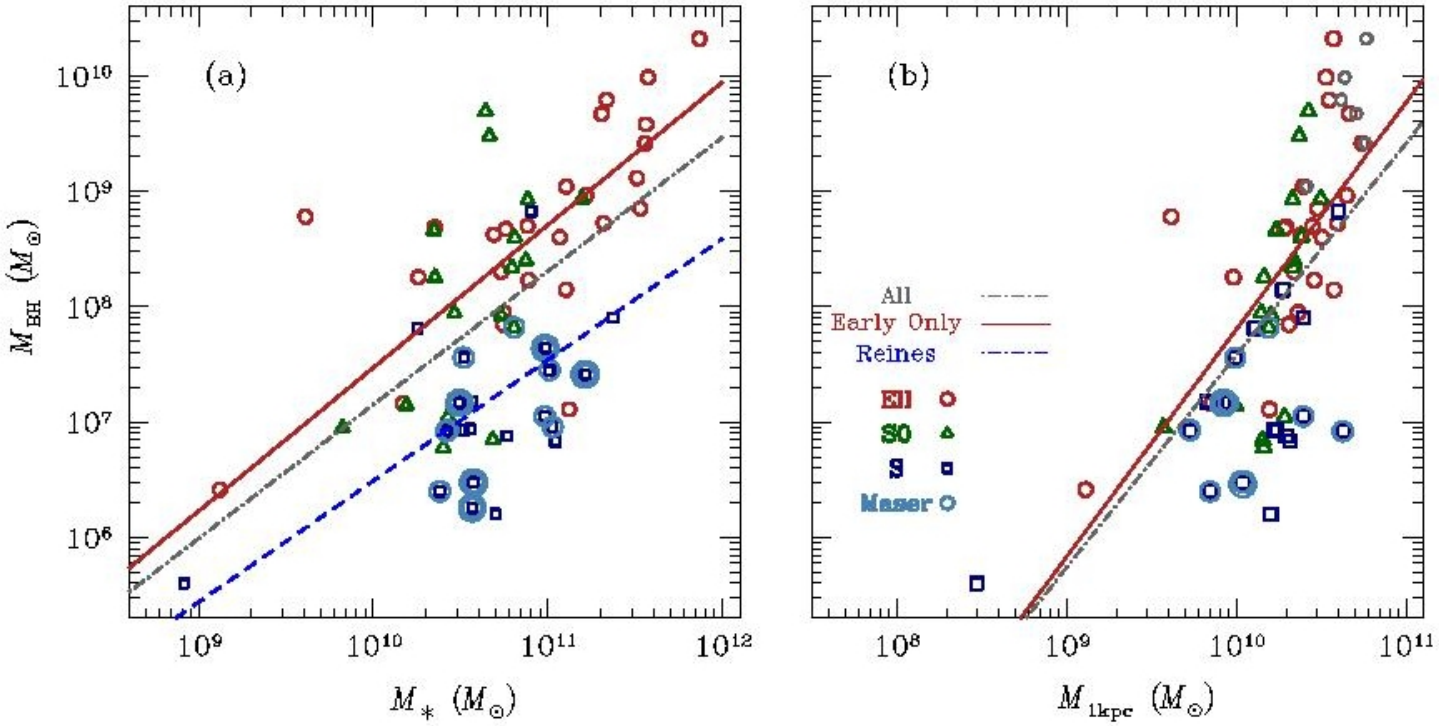

FIG. 2.— (**a**): Relationship between M_{BH} and M_*. We show elliptical (red circles), S0 (green triangles), spiral (blue squares), and megamaser disk (blue circles) galaxies. Double circles indicate our new measurements. We show fits to the full sample (grey dot-dashed), the early-types (red solid) and the Reines & Volonteri (2015) fit (blue dashed). (**b**): The relationship between M_{BH} and mass enclosed within 1 kpc. Symbols as at left. In grey we show the galaxy mass "corrected" for core-scouring (e.g., Rusli et al. 2013). Galaxies with radii <2" are excluded.

The same

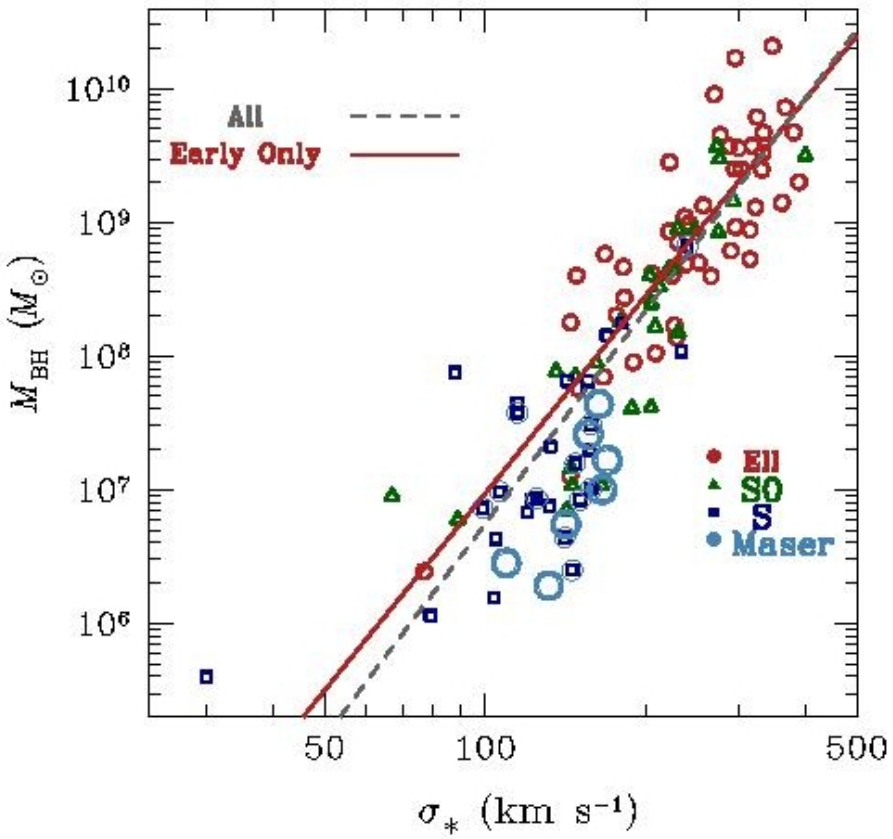

FIG. 3.— The relationship between σ_* and M_{BH}. We fit the entire sample (grey dashed line) and the early-type galaxies alone (red solid). Note the systematic offset to lower M_{BH} at a fixed σ_* for the megamaser disk galaxies. Symbols as in Figure 2.

Массы черных дыр в мегамазерах меньше!

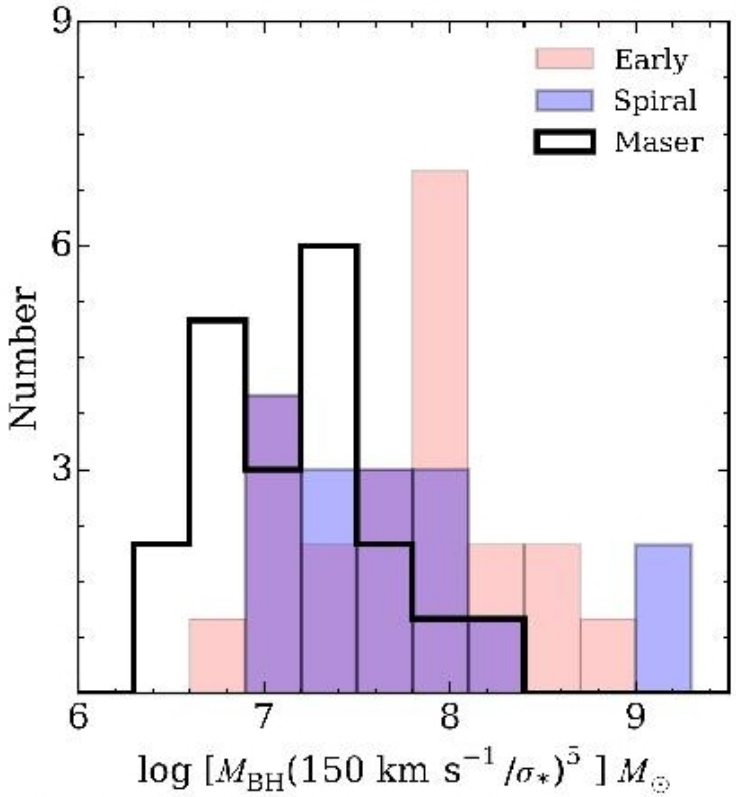

FIG. 4.— The distribution of M_{BH} at fixed σ_*. Megamaser galaxies (open) are offset to lower M_{BH} than the non-maser spirals (blue filled) or the early-type galaxies (red filled).

Astro-ph: 1605.09381

ALMA RESOLVES THE NUCLEAR DISKS OF ARP 220

Nick Scoville[1], Lena Murchikova[1], Fabian Walter[2], Catherine Vlahakis[3], Jin Koda[15], Paul Vanden Bout[10], Joshua Barnes[5,4], Lars Hernquist[6], Kartik Sheth[20], Min Yun[4], David Sanders[5], Lee Armus,[16], Pierre Cox,[17,18], Todd Thompson[13,14], Brant Robertson[11], Laura Zschaechner[2], Linda Tacconi[9], Paul Torrey,[19,7], Christopher C. Hayward[7], Reinhard Genzel[9], Phil Hopkins[1], Paul van der Werf[12], Roberto Decarli[2]

Draft version June 1, 2016

ABSTRACT

We present 90 mas (37 pc) resolution ALMA imaging of Arp 220 in the CO (1-0) line and continuum at $\lambda = 2.6$ mm. The internal gas distribution and kinematics of both galactic nuclei are well-resolved for the first time. In the more luminous West nucleus, the major gas and dust emission extends to $0.2''$ radius (80 pc); the central resolution element shows a strong peak in the dust emission but a factor 3 dip in the CO line emission. In this nucleus, the dust is apparently optically thick ($\tau_{2.6\mathrm{mm}} \sim 1$) at $\lambda = 2.6$ mm with a dust emission brightness temperature ~ 120 K. The column of ISM at this nucleus is $N_{H2} \geq 2 \times 10^{26}$ cm^{-2}, corresponding to $A_V = 10^6$ mag and 1000 gr cm^{-2}. The East nucleus is somewhat more elongated with radial extent $0.3''$ or ~ 120 pc. The derived kinematics of

Разрешение по скорости

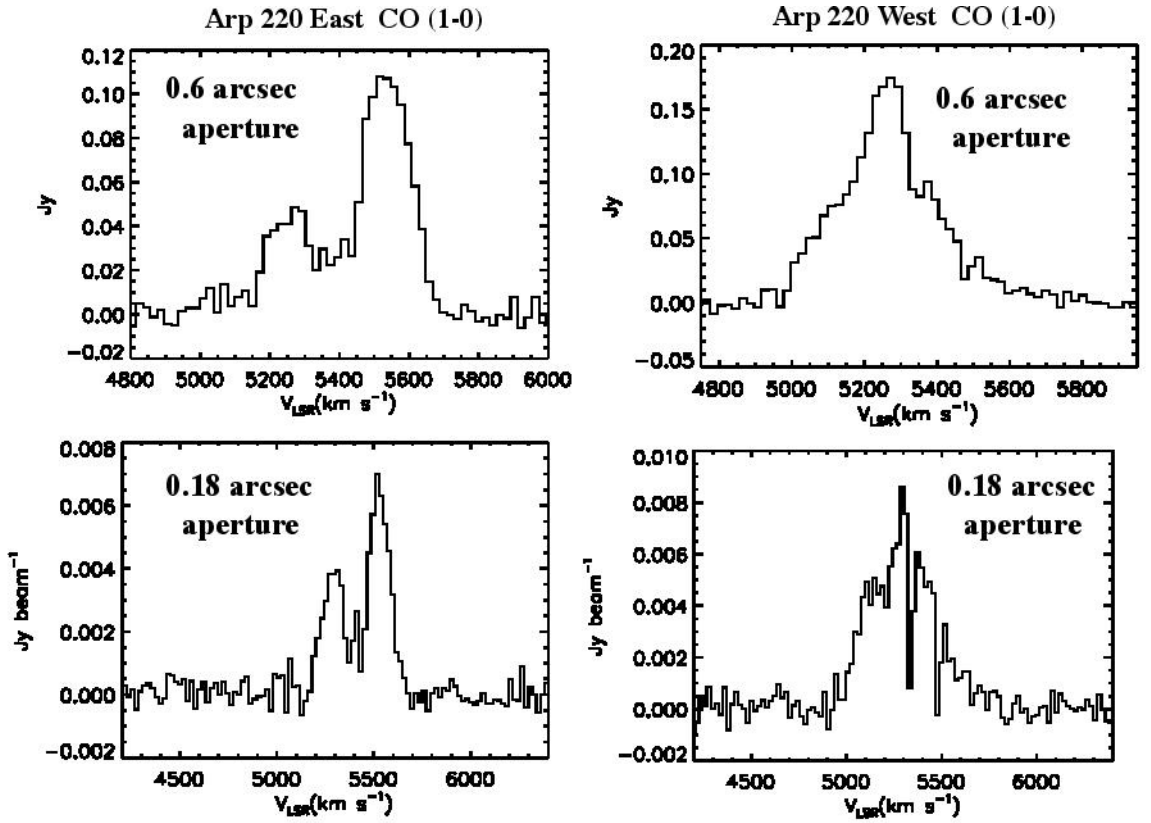

3. The CO (1-0) emission from the West and East nuclei, in apertures of 0.6 ″ (top panels) and 0.18 ″ (bottom panel

Разрешение пространственное

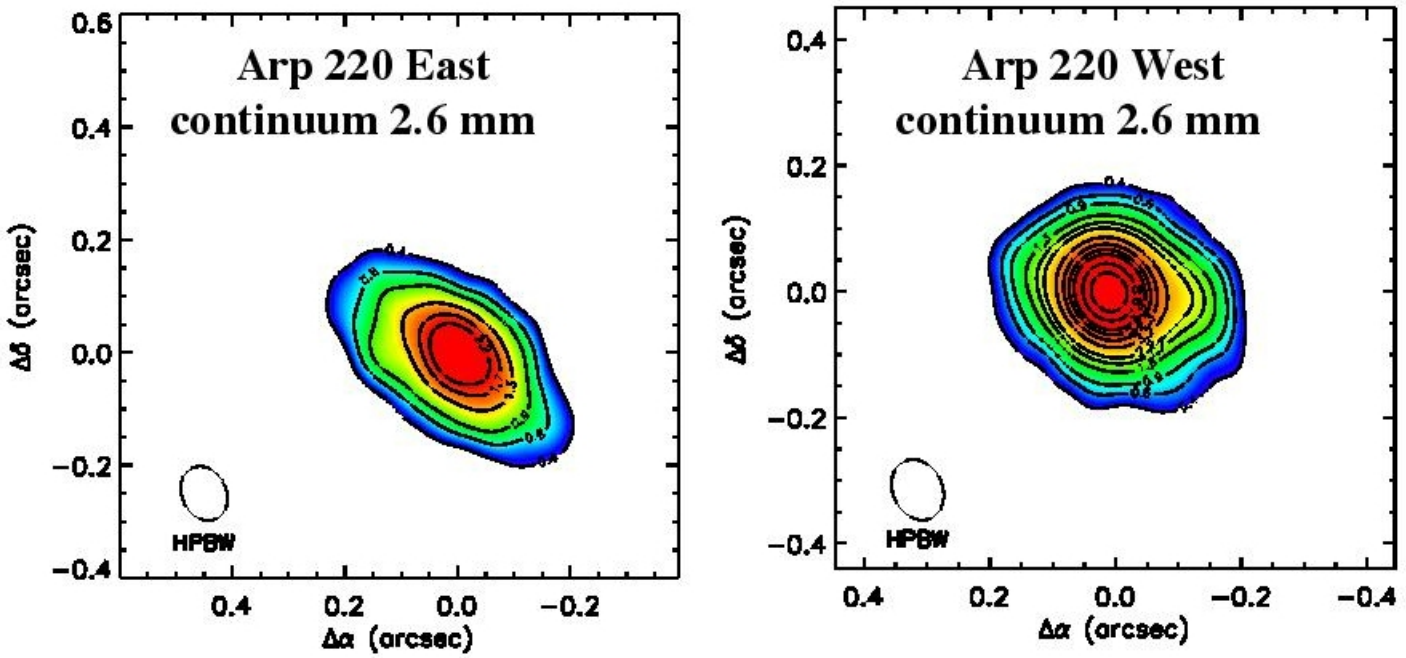

Figure 1. The 2.6 mm continuum distribution on the East and West nuclei is shown at $0.08 \times 0.1''$ resolution (33×41 pc) . The peak values are 2.5 (East) and 11.9 mJy beam^{-1} (West). Coordinate offsets are relative to the 2.6 mm continuum peaks (Table 1) and the contours are mJy beam^{-1}.

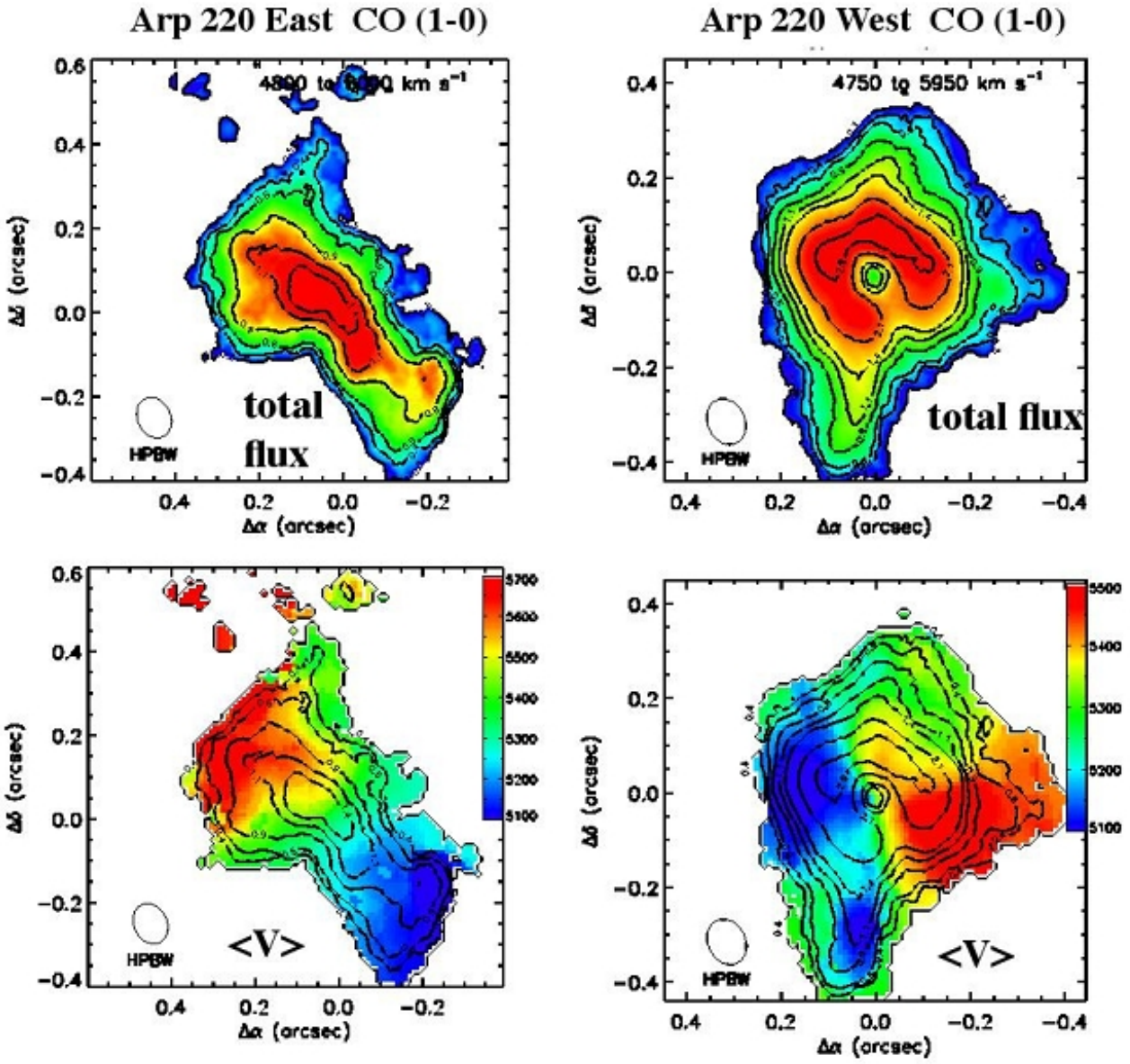
Arp 220 East CO (1-0)
Arp 220 West CO (1-0)
4750 to 5950 km s⁻¹
total flux
HPBW
<V>
Δδ (arcsec)
Δα (arcsec)

Кинематическая модель

Table 4
Nuclear Disk Emissivity and Kinematic Models

	West Nucleus	
Systemic velocity	V_{sys}	5434 km s^{-1}
Gas turbulence	FWHM Δv	250 km s^{-1}
Disk inclination	i	30°
Major axis	P.A.	265°
Rotation curve:	Point mass	$\sim 8 \times 10^8$ $M_\odot$
	Mass at < 80 pc	$\sim 10^9 M_\odot$
CO emissivity:	Peak	at R$<$ 5 pc
	Flat and 10× lower axisymmetric.	at R = 10 - 50 pc
	East Nucleus	
Systemic velocity	V_{sys}	5528 km s^{-1}
Gas turbulence	FWHM Δv	120 km s^{-1}
Disk inclination	i	45°
Major axis	P.A.	50°
Rotation curve:	Point mass	$< 10^8$ $M_\odot$
	Mass at < 130 pc	$\sim 10^9 M_\odot$
CO emissivity:	0	at R$<$ 5 pc
	Peak	at R$\sim$ 10 pc
	Falls a factor 2	out to 100 pc
	Receding side 2× brighter.	

Черная дыра есть только в западном ядре!

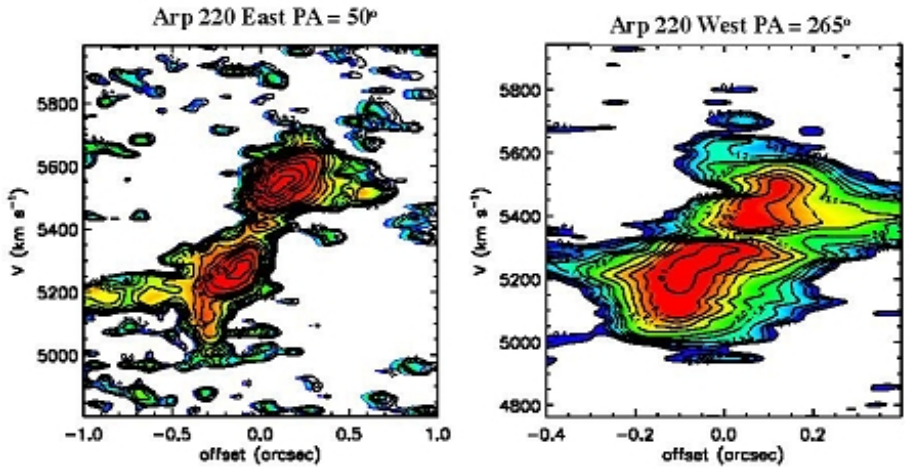

Figure 5. Spatial-velocity strip maps along the major axes of Arp 220 East (PA=50°) and West (PA = 265°). The coordinate offsets are measured relative to the 2.6 mm continuum peaks (see Figure 1). Positive offset coordinate corresponds to the receding (redshifted) side on the major axis i.e. for the West nucleus, positive offset is to the west and for the East nucleus, positive offset is northeast. Thus, on the West strip map (left panel), the emission at offset = -0.4″ and 5250 km s^{-1}is emission from the East nucleus coming in, and on the East strip map (right panel), the emission at offset < -0.5″ and 5200 km s^{-1}is the West nucleus coming in. The contours are labelled with mJy beam^{-1}.

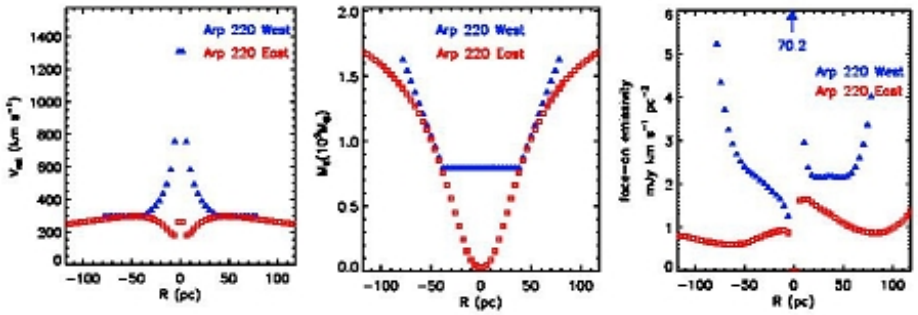

Figure 6. The derived rotation curves, enclosed dynamical mass (in a simple spherical approximation $M_R = RV_{rot}^2$) and face-on emissivity